crystals

MDPI

Article

Anomalous Positron Lifetime in Single Crystal of Weyl Semimetal CoSi

D. A. Salamatin [1,2], A. V. Bokov [1], M. G. Kozin [3], I. L. Romashkina [3], A. V. Salamatin [2], M. V. Mikhin [2], A. E. Petrova [4], V. A. Sidorov [1], A. V. Nikolaev [3], Z. Fisk [5] and A. V. Tsvyashchenko [1,*]

1 Vereshchagin Institute of High Pressure Physics, RAS, Troitsk, 108840 Moscow, Russia; dasalam@hppi.troitsk.ru (D.A.S.)
2 Joint Institute for Nuclear Research, 141980 Dubna, Russia
3 Skobeltsyn Institute of Nuclear Physics, Lomonosov MSU, 119991 Moscow, Russia
4 Lebedev Physical Institute, RAS, 119991 Moscow, Russia
5 Department of Physics and Astronomy, University of California, Irvine, CA 92697, USA
* Correspondence: tsvyash@hppi.troitsk.ru

Abstract: The positron annihilation lifetimes were measured using a ^{48}V positron source in noncentrosymmetric cubic single crystals of CoSi, FeSi and MnSi. The following lifetimes were determined from the positron annihilation time spectra: 168(1) ps for CoSi, 114(1) ps for FeSi and 111(1) ps for MnSi. For single-crystal CoSi, the positron annihilation lifetime was also determined with a ^{22}Na positron source. For CoSi, the lifetimes obtained from different positron sources are consistent. The differences in the positron annihilation lifetimes in MnSi and FeSi, on the one hand, and in the Weyl semimetal CoSi, on the other hand, are possibly caused by the formation of a positron + electron bound state (positronium).

Keywords: positron annihilation; ^{48}V positron source; single crystals; noncentrosymmetric structure B20

Citation: Salamatin, D.A.; Bokov, A.V.; Kozin, M.G.; Romashkina, I.L.; Salamatin, A.V.; Mikhin, M.V.; Petrova, A.E.; Sidorov, V.A.; Nikolaev, A.V.; Fisk, Z.; et al. Anomalous Positron Lifetime in Single Crystal of Weyl Semimetal CoSi. *Crystals* **2023**, *13*, 509. https://doi.org/10.3390/cryst13030509

Academic Editor: Sergey L. Bud'ko

Received: 2 February 2023
Revised: 9 March 2023
Accepted: 14 March 2023
Published: 16 March 2023

1. Introduction

Positronium (Ps) is a purely lepton bound state consisting of an electron and a positron [1,2]. As the simplest electromagnetically bound state, it is an ideal system for studying in quantum electrodynamics. Ps can exist either in a spin-singlet (para(p)–Ps) state or in a spin-triplet (ortho(o)–Ps) state. In vacuum, these states have an average lifetime of 0.125 ns and 142 ns, respectively [3,4]. The Ps lifetimes in solids differ from their values in vacuum due to the many-particle Coulomb interaction. For example, in the α-SiO_2 single crystal, the lifetime of p-Ps amounts to $\tau_{p-Ps} = 156(4)$ ps [5]. The formation of Ps both on the surface of a solid [6] and in the bulk [7] depends on the electronic structure near the Fermi level of the sample under study. In studying the formation of Ps in multilayer graphene, grown on a polycrystalline copper substrate, it has been found that Ps in graphene and Ps on the surface of copper are different [8]. On the other hand, it is well known that the electronic structure of graphene, characterized by the presence of quasi-two-dimensional Dirac fermions, gives rise to a discovery of Weyl semimetals that contain massless Dirac–Weyl fermions in three dimensions [9–14].

This suggests that the formation of Ps can also be expected in single crystals of Weyl semimetals, including, in particular, CoSi, RhSi, RhSn, and PtAl [15–19], which are crystallized in the noncentrosymmetric structure of the FeSi-type (the $P2_13$ space group). In addition, in these quantum materials, such unusual objects as chiral fermions have been found. For CoSi and RhSi, the existence of two types of chiral fermions with nonzero Chern numbers was confirmed: spin-1 and charge-2. Ab initio calculations [20] showed that their band structure near the Fermi energy (E_F) has a threefold degenerate point at the Γ point and a fourfold degenerate point at the R point of the Brillouin zone. It is also

worth mentioning that in CoSi and RhSi the topological superconductivity was theoretically predicted in Ref. [21]. New spin-related transport properties of these unconventional chiral fermionic semimetals make them very promising for future spintronic and spin caloritronics applications [22], while the quantum combination of topological and optical properties can be used for new information technologies [23].

The electronic properties of CoSi are often compared with those of MnSi and FeSi. Notice that, since Mn, Fe and Co are consecutive elements of the same row in the periodic table, in going from Mn to Fe and then to Co, the 3*d* electron band acquires more electrons and the Fermi energy (E_F) is increased. As a result, in FeSi, the added electron populates the unoccupied states below the energy gap, while in CoSi the extra electron is accommodated by filling electron states above the gap, with E_F reaching a three-fold degenerate state at the Γ point and a four-fold degenerate level at the *R* point [24]. Correspondingly, one observes a change in properties from the helicoid magnet MnSi [25] through the formation of the Kondo state in FeSi [26] to the chiral diamagnetic Weyl semimetal ground state in CoSi. This change, caused by differences in the electronic band structure near the Fermi level, can be probed by positron annihilation, and, in this paper, we present our results of the positron lifetime annihilation spectroscopy (PALS) study performed in CoSi, FeSi, and MnSi single crystals.

Usually, the positron annihilation rate (inversely proportional to the annihilation lifetime τ) is determined by the overlap of the positron $\rho_+(r) = |\psi_+(r)|^2$ and electron $\rho_-(r)$ densities in the localization region: $\lambda = \frac{1}{\tau} = \pi r_0^2 c \int |\psi_+(r)|^2 \rho_-(r) \gamma dr$, where r_0 is the classical electron radius, whereas $\gamma = \gamma[\rho_-(r)] = 1 + \frac{\Delta\rho_-}{\rho_-}$ describes the increase in the electron density as a result of the mutual Coulomb attraction of the electron and the positron [27]. For performing PALS experiments in laboratories, the preferred source of positrons is usually ^{22}NaCl on thin metal (Ni, Al) or polymer foil (Kapton, Mylar). However, the monosilicides MnSi, FeSi and CoSi have already been studied using this source or accelerator beams [28–31]. In this work, as a source of positrons, we have decided to use the ^{48}V isotope in titanium foil with a half-life $T_{1/2} \approx 16$ days, which makes PALS measurements more convenient and environmentally friendly. First, titanium has a high melting point (1668 °C), which makes it possible to use the obtained source in various experiments at high temperatures (for example, in liquid metals or boiling solutions). On the other hand, at low temperatures, this source is also convenient in experiments due to its low thermal conductivity (13 times less than the thermal conductivity of aluminum and 4 times less than that of iron), making it possible to carry out positron measurements with high accuracy in a thermostat, and also without the possibility of dissolving the source itself in the process of its operation. A chemically aggressive environment (for example, molten salts) is also not a problem for such a source due to the high corrosion resistance of titanium. Due to its convenient shape (thin metal foil), ^{48}V can also be used in high pressure experiments. Secondly, after titanium foil irradiation at the cyclotron, active nuclides ^{48}V are distributed in the titanium node, and the foil becomes a closed source of positrons, which is already ready for experiments without requiring radiochemical preparation. This allows you not to worry about additional personal protective equipment in the future due to the fact that the source will be lost or smeared on the surfaces of other materials. Moreover, the relatively short half-life makes it possible to store the source without excessive radiation and biological protection almost immediately after its use in a nuclear physics experiment. Based on this, excessive environmental pollution does not occur, and the process of "recharging" the source can be easily controlled by having a cyclotron with a beam of low-energy protons. Compared to ^{22}Na, the positron spectrum from ^{48}V has higher energy, with a maximum of about 700 keV (for ^{22}Na, the maximum energy is 545 keV). A higher positron energy will make it possible to study slightly thicker layers of the studied substance (and hence the volume) and is commensurate with the energies of the ^{22}Na source; thus, it does not require additional serious changes in the reconfiguration of the experimental technique and changes in the design of the detectors (replacement of crystals and the electronic part of the equipment).

2. Materials and Methods

The samples of MnSi ($a = 4.5598(2)$ Å) and CoSi ($a = 4.444(1)$ Å) single crystals studied in this work were grown by the Bridgman method [32,33] (Ames Laboratory), and their crystal structure was well defined and they have been characterized by various macroscopic measurements (see [32–34]). The sample of FeSi ($a = 4.486(2)$ Å) single crystal was grown by the Czochralski method. The lattice parameters of the crystals, determined by X-ray diffraction, correspond well to literature data [33,35,36]. As has been mentioned earlier, as a source of positrons, we used the ^{48}V isotope obtained by the reaction ^{48}Ti(p,n)^{48}V by irradiating titanium foil (50 μm) with protons with an energy of 7.8 MeV (in the cyclotron of the Institute of Nuclear Physics, Moscow State University). The scattering cross section for protons was about 65 mbarn [37,38]. The use of relatively low proton energy proved to be sufficient to obtain the required ^{48}V activity. Measurements of the energy spectrum of the irradiated foil showed the absence of "spurious" lines from another isotope (see Figure 1).

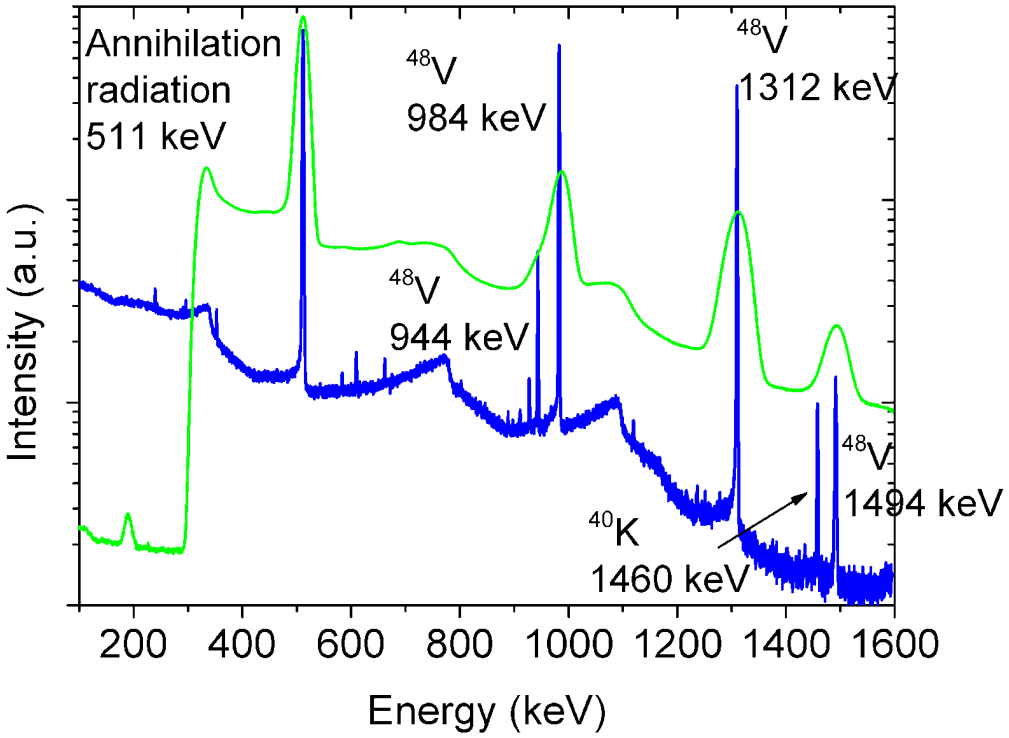

Figure 1. Measured energy spectrum of an irradiated 50 μm thick titanium foil. The blue points are data from the HPGe detector, and the green points are data from the $LaBr_3$:Ce detector.

Annihilation time spectra with the ^{48}V positron source were measured using the "VUKAP" four-detector compact digital spectrometer equipped with two $LaBr_3$:Ce detectors (BrilLanCe^{TM} 380) [39]. The time resolution of the spectrometer (FWHM at ^{60}Co) was 380 ps. Two detectors were installed at an angle of 90° to each other at a short distance. The irradiated titanium foil was sandwiched between two samples of the same single crystal. Such a "sandwich" was installed at an angle of 45° to the detectors. All measurements were carried out at room temperature using the same positron source. The source size was 5×5 mm^2, which made it possible to completely cover the source with samples. The initial activity of the source was about 150 kBq. The 1312 keV γ-ray photon from the ^{48}V decay was used for the "START" and the 511 keV annihilation gamma-ray photon for the "STOP". Each PALS spectrum contained more than 6 million counts.

3. Results and Discussion

The time spectra of bulk positron annihilation and their characteristics, described with the two-exponential model in the LT10 program [40], are shown in Figure 2 and in Table 1. Our results for MnSi and FeSi agree with previous measurements performed with other experimental setups with ^{22}Na as a positron source [29,31]. It has been found that the value of τ for the second component varies from 1700 ps to 4000 ps depending on the sample under study. Therefore, we attribute the second component to the medium between the samples and the source. Its partial contribution to the intensity varies from 0.5% to 3%. The intensity contribution from the annihilation in the source (the 50 μm width Ti foil) should be within 15–20% [41]. As pointed out in [42], the main component (about 90%) from a proton-irradiated unannealed Ti-foil source is described by $\tau \approx 37$ ps. We were unable to resolve such a low lifetime due to the finite time resolution of the spectrometer. As a result, the contribution of the positron source to the spectra could not be reliably determined. We then measured the PALS spectrum for the CoSi single crystal using another spectrometer with a time resolution of about 200 ps and the ^{22}NaCl positron source (Joint Institute for Nuclear Research, Dubna). In this case, the positron lifetime is 166(2) ps (see Figure 3 and Table 1), which coincides with the result obtained with a ^{48}V positron source. We also measured the PALS spectrum for the Si single crystal with a ^{48}V positron source. The positron lifetime is 218(1) ps (see Figure 3 and Table 1), which coincides with the result obtained with a ^{48}V positron source [43]. The lifetimes for MnSi and FeSi are found to be approximately the same, despite the different densities of electron states at E_F. While MnSi is a metal, FeSi has a small energy gap of about 75 μeV above the filled electron band. On the other hand, our high-quality single crystal positron annihilation lifetime in CoSi has turned out to be 1.5 times larger than the found values of τ in MnSi, FeSi and polycrystal CoSi (see Figure 2 and Table 1). This result contradicts the previous value of the positron lifetime, obtained in polycrystalline samples of CoSi [28]. According to Ref. [28], the lifetime in polycrystalline CoSi amounts to 115 ps, which is close to the value of τ both in the MnSi single crystal (Table 1) and in FeSi and apparently can be explained by positron annihilation on conducting electrons, despite the fact that defects may exist in a polycrystalline sample of CoSi. In our case, we consider that the positron annihilation in the single-crystal CoSi can be associated with its electronic features [17,44]. In particular, since the chiral Weyl fermions near the Fermi energy are absent in MnSi and FeSi, their presence can probably account for the formation and subsequent decay of the Ps, which results in a longer positron annihilation lifetime observed experimentally. The peculiarities of CoSi in this B20-compounds row have been recently observed on the temperature dependence of elastic constants; the values of c_{11} and c_{12} are highest for CoSi and then follow FeSi and MnSi [33,45]. In contrast to FeSi, inelastic neutron scattering measurements have shown that CoSi exhibits normal phonon behavior, which is clear from its different electronic structure [46]. Our experimental results certainly indicate the need for further research to elucidate the mechanism of positron annihilation in topological semimetal single crystals with Weyl singular points.

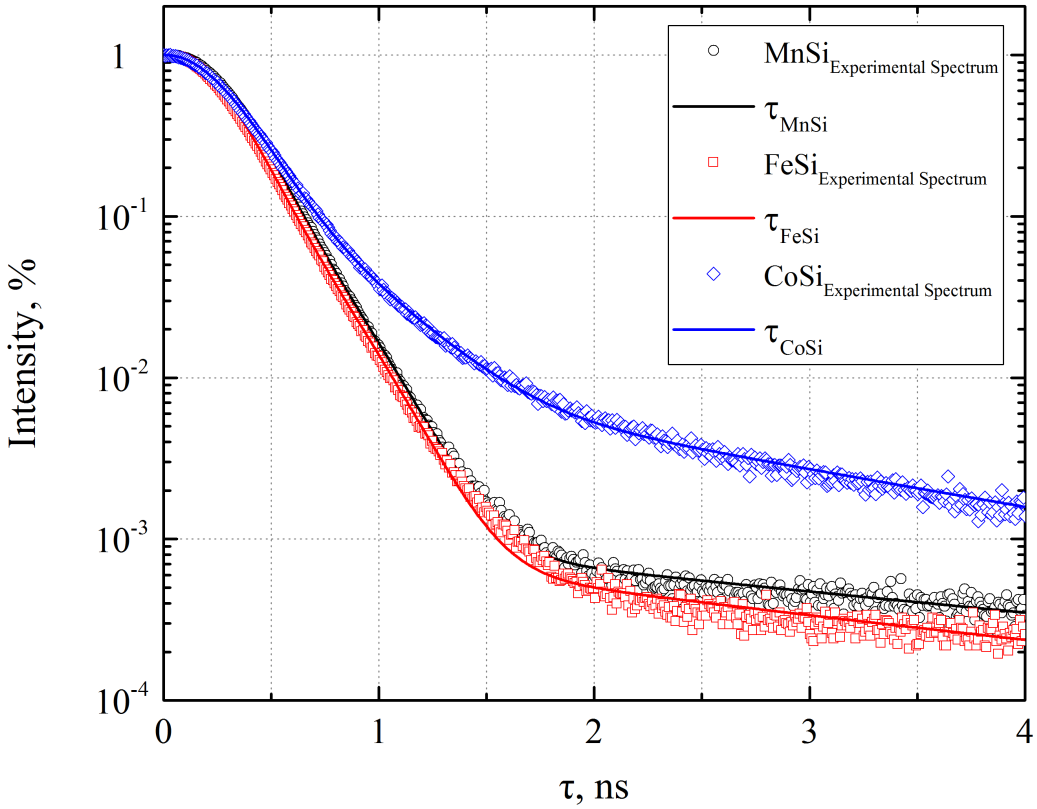

Figure 2. Time spectra of positron annihilation with the ^{48}V source in titanium foil and their fittings for the CoSi, MnSi, and FeSi single crystals.

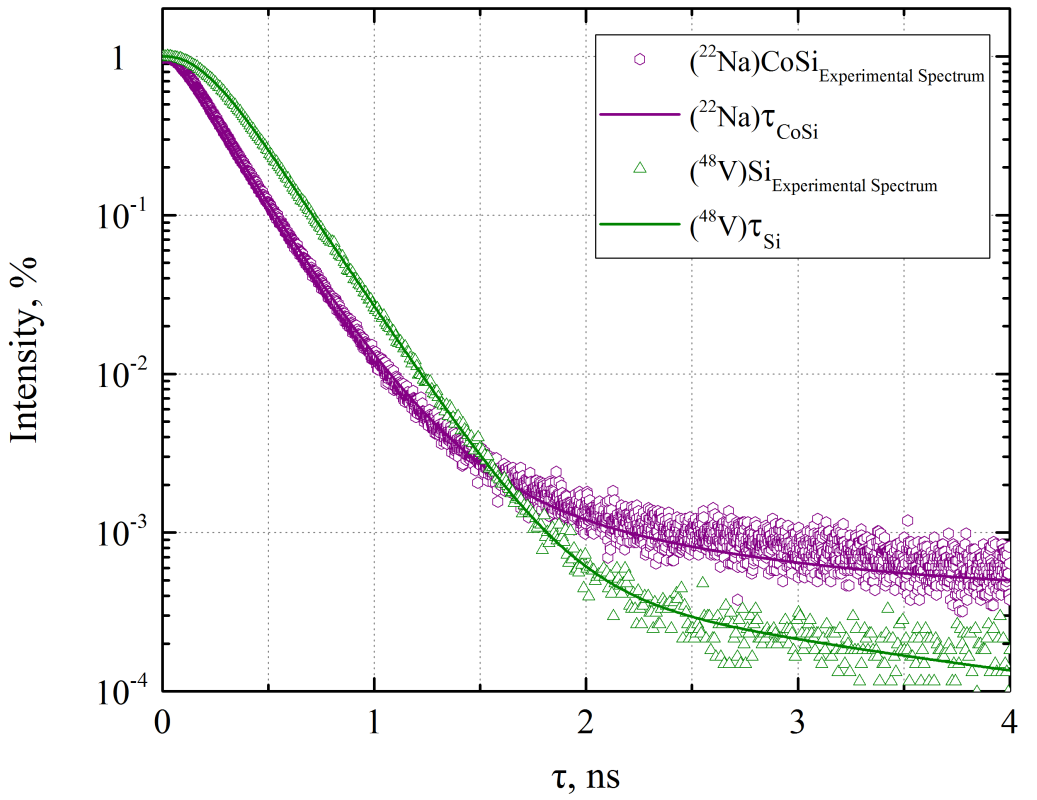

Figure 3. Time spectra of positron annihilation for the CoSi single crystal with the ^{22}Na source and for the Si single crystal with the ^{48}V source.

Table 1. Measured positron annihilation lifetimes (τ_{exp}) in single crystals of Si, CoSi, MnSi, and FeSi (this work), compared with τ_b in polycristalline samples (CoSi, MnSi, FeSi) and the Si single crystal with ^{22}Na as a source of positrons.

Material	τ_{exp}, ps (in This Work)	τ_b, ps (According to Literature)
Si	218(1) (with ^{48}V)	218(1) (single crystal) [43]
CoSi	168(1) (with ^{48}V), 166(2) (with ^{22}Na)	115(2) (polycrystal) [28]
FeSi	114(1) (with ^{48}V)	130(3) (polycrystal) [31]
MnSi	111(1) (with ^{48}V)	119(3) (single crystal) [29]

4. Conclusions

Our measurements of the PALS spectra in the single crystals of MnSi, FeSi and CoSi indicate that the positron annihilation lifetime in CoSi is approximately 1.5 times longer than τ in MnSi and FeSi, and by the same amount exceeds the value of τ, obtained in polycrystalline CoSi. The longer lifetime implies a possible formation of the Ps. The peculiarities of CoSi in this B20-compounds row also have been recently observed on the temperature dependence of elastic constants, the small value of shear modulo and phonon density of states.

In the future, we plan to continue our PALS study of other topological Weyl semimetals at various temperatures. In addition, we prepare the PALS experiment at high pressure thanks to the good possibilities of the ^{48}V positron source.

Author Contributions: Conceptualization, A.V.T.; methodology, D.A.S., A.V.S., M.V.M., M.G.K. and I.L.R.; software, D.A.S. and M.V.M.; formal analysis, A.V.B.; investigation, D.A.S., M.G.K., I.L.R. and A.V.T.; resources, A.E.P., V.A.S. and Z.F.; data curation, D.A.S.; writing—original draft preparation, A.V.T.; writing—review and editing, D.A.S., A.V.B., M.G.K. and I.L.R.; visualization, D.A.S. and A.V.B.; supervision, A.V.T. and A.V.N.; project administration, A.V.T. All authors have read and agreed to the published version of the manuscript.

Funding: The study was supported by the Russian Science Foundation Grant No. 22-12-00008 (https://rscf.ru/project/22-12-00008/accessed on 1 February 2023).

Data Availability Statement: The data presented in this study are available on request from the corresponding author.

Acknowledgments: The authors are grateful to Pawel Horodek for the help in conducting PALS measurements with ^{22}Na positron source, Sergei Mikhailovich Stishov for providing the samples and Dmitry Olegovich Eremenko for help in fabricating the positron source. We thank Vadim Veniaminovich Brazhkin for his support of the work and for his valuable remarks.

Conflicts of Interest: The authors declare no conflict of interest.

Abbreviations

The following abbreviations are used in this manuscript:

Ps	positronium
PAL	positron annihilation lifetime
PALS	positron annihilation lifetime spectroscopy

References

1. Mohorovičić, S. Möglichkeit neuer Elemente und ihre Bedeutung für die Astrophysik. *Astron. Nachr.* **1934**, *253*, 93–108. [CrossRef]
2. Deutsch, M. Evidence for the Formation of Positronium in Gases. *Phys. Rev.* **1951**, *82*, 455–456. [CrossRef]
3. Al-Ramadhan, A.H.; Gidley, D.W. New precision measurement of the decay rate of singlet positronium. *Phys. Rev. Lett.* **1994**, *72*, 1632–1635. [CrossRef] [PubMed]
4. Asai, S.; Orito, S.; Shinohara, N. New measurement of the orthopositronium decay rate. *Phys. Lett. B* **1995**, *357*, 475–480. [CrossRef]

5. Saito, H.; Hyodo, T. Direct Measurement of the Parapositronium Lifetime in α-SiO_2. *Phys. Rev. Lett.* **2003**, *90*, 193401. [CrossRef] [PubMed]
6. Mills, A.P.; Pfeiffer, L.; Platzman, P.M. Positronium Velocity Spectroscopy of the Electronic Density of States at a Metal Surface. *Phys. Rev. Lett.* **1983**, *51*, 1085–1088. [CrossRef]
7. Nagai, Y.; Kakimoto, M.; Hyodo, T.; Fujiwara, K.; Ikari, H.; Eldrup, M.; Stewart, A.T. Temperature dependence of the momentum distribution of positronium in MgF_2, SiO_2, and H_2O. *Phys. Rev. B* **2000**, *62*, 5531–5535. [CrossRef]
8. Chirayath, V.A.; Fairchild, A.J.; Gladen, R.W.; Chrysler, M.D.; Koymen, A.R.; Weiss, A.H. Positronium formation in graphene and graphite. *Aip Conf. Proc.* **2019**, *2182*, 050002. [CrossRef]
9. Wang, Z.; Sun, Y.; Chen, X.Q.; Franchini, C.; Xu, G.; Weng, H.; Dai, X.; Fang, Z. Dirac semimetal and topological phase transitions in A_3Bi (A = Na, K, Rb). *Phys. Rev. B* **2012**, *85*, 195320. [CrossRef]
10. Wang, Z.; Weng, H.; Wu, Q.; Dai, X.; Fang, Z. Three-dimensional Dirac semimetal and quantum transport in Cd_3As_2. *Phys. Rev. B* **2013**, *88*, 125427. [CrossRef]
11. Neupane, M.; Xu, S.Y.; Sankar, R.; Alidoust, N.; Bian, G.; Liu, C.; Belopolski, I.; Chang, T.R.; Jeng, H.T.; Lin, H.; et al. Observation of a three-dimensional topological Dirac semimetal phase in high-mobility Cd_3As_2. *Nat. Commun.* **2014**, *5*, 3786. [CrossRef]
12. Borisenko, S.; Gibson, Q.; Evtushinsky, D.; Zabolotnyy, V.; Büchner, B.; Cava, R.J. Experimental Realization of a Three-Dimensional Dirac Semimetal. *Phys. Rev. Lett.* **2014**, *113*, 027603. [CrossRef]
13. Liu, Z.K.; Zhou, B.; Zhang, Y.; Wang, Z.J.; Weng, H.M.; Prabhakaran, D.; Mo, S.K.; Shen, Z.X.; Fang, Z.; Dai, X.; et al. Discovery of a Three-Dimensional Topological Dirac Semimetal, Na_3Bi. *Science* **2014**, *343*, 864–867. [CrossRef]
14. Xu, S.Y.; Belopolski, I.; Alidoust, N.; Neupane, M.; Bian, G.; Zhang, C.; Sankar, R.; Chang, G.; Yuan, Z.; Lee, C.C.; et al. Discovery of a Weyl fermion semimetal and topological Fermi arcs. *Science* **2015**, *349*, 613–617. [CrossRef]
15. Rao, Z.; Li, H.; Zhang, T.; Tian, S.; Li, C.; Fu, B.; Tang, C.; Wang, L.; Li, Z.; Fan, W.; et al. Observation of unconventional chiral fermions with long Fermi arcs in CoSi. *Nature* **2019**, *567*, 496–499. [CrossRef] [PubMed]
16. Sanchez, D.S.; Belopolski, I.; Cochran, T.A.; Xu, X.; Yin, J.X.; Chang, G.; Xie, W.; Manna, K.; Süß, V.; Huang, C.Y.; et al. Topological chiral crystals with helicoid-arc quantum states. *Nature* **2019**, *567*, 500–505. [CrossRef]
17. Takane, D.; Wang, Z.; Souma, S.; Nakayama, K.; Nakamura, T.; Oinuma, H.; Nakata, Y.; Iwasawa, H.; Cacho, C.; Kim, T.; et al. Observation of Chiral Fermions with a Large Topological Charge and Associated Fermi-Arc Surface States in CoSi. *Phys. Rev. Lett.* **2019**, *122*, 076402. [CrossRef] [PubMed]
18. Li, H.; Xu, S.; Rao, Z.C.; Zhou, L.Q.; Wang, Z.J.; Zhou, S.M.; Tian, S.J.; Gao, S.Y.; Li, J.J.; Huang, Y.B.; et al. Chiral fermion reversal in chiral crystals. *Nat. Commun.* **2019**, *10*, 5505. [CrossRef] [PubMed]
19. Schröter, N.B.M.; Pei, D.; Vergniory, M.G.; Sun, Y.; Manna, K.; de Juan, F.; Krieger, J.A.; Süss, V.; Schmidt, M.; Dudin, P.; et al. Chiral topological semimetal with multifold band crossings and long Fermi arcs. *Nat. Phys.* **2019**, *15*, 759–765. [CrossRef]
20. Tang, P.; Zhou, Q.; Zhang, S.C. Multiple Types of Topological Fermions in Transition Metal Silicides. *Phys. Rev. Lett.* **2017**, *119*, 206402. [CrossRef]
21. Lee, C.; Yoon, C.; Kim, T.; Chung, S.B.; Min, H. Topological multiband s-wave superconductivity in coupled multifold fermions. *Phys. Rev. B* **2021**, *104*, L241115. [CrossRef]
22. Hsieh, T.Y.; Prasad, B.B.; Guo, G.Y. Helicity-tunable spin Hall and spin Nernst effects in unconventional chiral fermion semimetals XY (X = Co, Rh; Y = Si, Ge). *Phys. Rev. B* **2022**, *106*, 165102. [CrossRef]
23. Castelvecchi, D. The strange topology that is reshaping physics. *Nature* **2017**, *547*, 272–274. [CrossRef] [PubMed]
24. Pshenay-Severin, D.A.; Burkov, A.T. Electronic Structure of B20 (FeSi-Type) Transition-Metal Monosilicides. *Materials* **2019**, *12*, 2710. [CrossRef] [PubMed]
25. Mühlbauer, S.; Binz, B.; Jonietz, F.; Pfleiderer, C.; Rosch, A.; Neubauer, A.; Georgii, R.; Böni, P. Skyrmion Lattice in a Chiral Magnet. *Science* **2009**, *323*, 915–919. [CrossRef]
26. Schlesinger, Z.; Fisk, Z.; Zhang, H.T.; Maple, M.B.; DiTusa, J.; Aeppli, G. Unconventional charge gap formation in FeSi. *Phys. Rev. Lett.* **1993**, *71*, 1748–1751. [CrossRef]
27. Eldrup, M. Positron Methods for the Study of Defects in Bulk Materials. *J. Phys. IV France* **1995**, *05*, C1-93–C1-109. [CrossRef]
28. Abhaya, S.; Amarendra, G. Positron annihilation studies on bulk cobalt silicides. *Phys. Status Solidi C* **2009**, *6*, 2519–2522. [CrossRef]
29. Reiner, M.; Bauer, A.; Leitner, M.; Gigl, T.; Anwand, W.; Butterling, M.; Wagner, A.; Kudejova, P.; Pfleiderer, C.; Hugenschmidt, C. Positron spectroscopy of point defects in the skyrmion-lattice compound MnSi. *Sci. Rep.* **2016**, *6*, 29109. [CrossRef]
30. Mostafaa, K.; De Baerdemaekera, J.; Calvillob, P.; Van Caenegemb, N.; Houbaertb, Y.; Segers, D. A Study of Defects in Iron Based Alloys by Positron Annihilation Techniques. *Acta Phys. Pol. A* **2008**, *113*, 1471–1478. [CrossRef]
31. Bharathi, A.; Hariharan, Y.; Mani, A.; Sundar, C.S. Positron-lifetime studies in the Kondo insulator FeSi. *Phys. Rev. B* **1997**, *55*, R13385–R13388. [CrossRef]
32. Stishov, S.M.; Petrova, A.E.; Khasanov, S.; Panova, G.K.; Shikov, A.A.; Lashley, J.C.; Wu, D.; Lograsso, T.A. Magnetic phase transition in the itinerant helimagnet MnSi: Thermodynamic and transport properties. *Phys. Rev. B* **2007**, *76*, 052405. [CrossRef]
33. Petrova, A.E.; Krasnorussky, V.N.; Shikov, A.A.; Yuhasz, W.M.; Lograsso, T.A.; Lashley, J.C.; Stishov, S.M. Elastic, thermodynamic, and electronic properties of MnSi, FeSi, and CoSi. *Phys. Rev. B* **2010**, *82*, 155124. [CrossRef]
34. Stishov, S.M.; Petrova, A.E. Itinerant helimagnet MnSi. *Phys. Uspekhi* **2011**, *54*, 1117. [CrossRef]

35. Sales, B.C.; Jones, E.C.; Chakoumakos, B.C.; Fernandez-Baca, J.A.; Harmon, H.E.; Sharp, J.W.; Volckmann, E.H. Magnetic, transport, and structural properties of $Fe_{1-x}Ir_xSi$. *Phys. Rev. B* **1994**, *50*, 8207–8213. [CrossRef]
36. Wong-Ng, W.; McMurdie, F.H.; Paretzkin, B.; Zhang, Y.; Davis, K.L.; Hubbard, C.R.; Dragoo, A.L.; Stewart, J.M. Reference X-ray diffraction powder patterns of fifteen ceramic phases. *Powder Diffr.* **1987**, *2*, 257–265. [CrossRef]
37. Khandaker, M.; Kim, K.; Lee, M.; Kim, K.; Kim, G.; Cho, Y.; Lee, Y. Investigations of the natTi(p,x)43,44m,44g,46,47,48Sc,48V nuclear processes up to 40 MeV. *Appl. Radiat. Isot.* **2009**, *67*, 1348–1354. 6th International Conference on Isotopes. [CrossRef]
38. Garrido, E.; Duchemin, C.; Guertin, A.; Haddad, F.; Michel, N.; Métivier, V. New excitation functions for proton induced reactions on natural titanium, nickel and copper up to 70 MeV. *Nucl. Instrum. Methods Phys. Res. Sect. B Beam Interact. Mater. Atoms* **2016**, *383*, 191–212. [CrossRef]
39. Salamatin, D.; Tsvyashchenko, A.; Salamatin, A.; Velichkov, A.; Magnitskaya, M.; Chtchelkatchev, N.; Sidorov, V.; Fomicheva, L.; Mikhin, M.; Kozin, M.; et al. Hyperfine field studies of the high-pressure phase of noncentrosymmetric superconductor RhGe (B20) doped with hafnium. *J. Alloys Compd.* **2021**, *850*, 156601. [CrossRef]
40. Giebel, D.; Kansy, J. LT10 Program for Solving Basic Problems Connected with Defect Detection. *Phys. Procedia* **2012**, *35*, 122–127. Positron Studies of Defects 2011. [CrossRef]
41. Krsjak, V.; Degmova, J.; Noga, P.; Petriska, M.; Sojak, S.; Saro, M.; Neuhold, I.; Slugen, V. Application of Positron Annihilation Spectroscopy in Accelerator-Based Irradiation Experiments. *Materials* **2021**, *14*, 6238. [CrossRef] [PubMed]
42. Dryzek, J. Positron source based on the ^{48}V isotope dedicated to positron lifetime spectroscopy. *Phys. Status Solidi C* **2009**, *6*, 2380–2383. [CrossRef]
43. Dannefaer, S.; Puff, W.; Kerr, D. Positron line-shape parameters and lifetimes for semiconductors: Systematics and temperature effects. *Phys. Rev. B* **1997**, *55*, 2182–2187. [CrossRef]
44. Xu, X.; Wang, X.; Cochran, T.A.; Sanchez, D.S.; Chang, G.; Belopolski, I.; Wang, G.; Liu, Y.; Tien, H.J.; Gui, X.; et al. Crystal growth and quantum oscillations in the topological chiral semimetal CoSi. *Phys. Rev. B* **2019**, *100*, 045104. [CrossRef]
45. Stishov, S.M.; Petrova, A.E. Thermodynamic, elastic and electronic properties of substances with chiral crystal structure: MnSi, FeSi, CoSi. *Phys. Uspekhi* **2021**, *65*. [CrossRef]
46. Delaire, O.; Marty, K.; Stone, M.B.; Kent, P.R.C.; Lucas, M.S.; Abernathy, D.L.; Mandrus, D.; Sales, B.C. Phonon softening and metallization of a narrow-gap semiconductor by thermal disorder. *Proc. Natl. Acad. Sci. USA* **2011**, *108*, 4725–4730. [CrossRef]